

# Prospective and retrospective coding in cortical neurons

Simon Brandt,  
Mihai Alexandru Petrovici, Walter Senn,  
Katharina Anna Wilmes\*, Federico Benitez\*  
*Department of Physiology, University of Bern, Switzerland*

\* Joint senior authorship

May 24, 2024

## Abstract

Brains can process sensory information from different modalities at astonishing speed; this is surprising as already the integration of inputs through the membrane causes a delayed response. Neuronal recordings *in vitro* reveal a possible explanation for the fast processing through an advancement of the output firing rates of individual neurons with respect to the input, a concept which we refer to as prospective coding. The underlying mechanisms of prospective coding, however, is not completely understood. We propose a mechanistic explanation for individual neurons advancing their output on the level of single action potentials and instantaneous firing rates. Using the Hodgkin-Huxley model, we show that the spike generation mechanism can be the source for prospective (advanced) or retrospective (delayed) responses with respect the underlying somatic voltage. A simplified Hodgkin-Huxley model identifies the sodium inactivation as a source for the prospective firing, controlling the timing of the neuron's output as a function the voltage and its derivative. We also consider a slower spike-frequency adaptation as a mechanisms that generates prospective firings to inputs that undergo slow temporal modulations. In general, we show that adaptation processes at different time scales can cause advanced neuronal responses to time-varying inputs that are modulated on the corresponding time scales.

## 1 Introduction

Humans and other animals must adapt their behavior to a complex and dynamic world of physical and social interactions. Adequately navigating our environments requires not only fast processing of external information, e.g., in the form of accurate real-time sensory perception, but arguably also the anticipation of future states. Our brains are the result of these strong evolutionary pressures, and can process sensory information from different modalities at astonishing speed; this is surprising, as the integration of inputs through layers of neurons should cause a delayed response. Thus, already at the level of basic perception we can point out a conceptual issue regarding the brain's processing speed, namely that signal transmission and synaptic/membrane integration introduce delays that, absent any other mechanisms, lead to slow signal processing. Prospective coding provides an elegant solution to these challenges. Prospectivity implies that neuronal activity at the present time represents expected future events. While there is experimental evidence that the brain can process information faster than the many forms of delay incurred by neuronal networks would suggest, a general interpretation of these findings in the light of prospective coding and its implementations for cortical computation is so far missing.

An important yet understudied possibility is that prospective coding takes place at the level of individual neurons (Brea et al., 2016), as opposed to be a collective phenomenon of populations of neurons. Cortical computation would greatly benefit from looking ahead in time to compensate neuronal delays, as shown by the recently development of prospective coding frameworks such as neuronal least action (NLA, Senn et al., 2024), latent equilibrium (LE, Haider et al., 2021), and generalized latent equilibrium (GLE, Ellenberger et al., 2024). All these methods share the assumption of prospective coding at the level of individual neurons, which predict the future state based on the current state and its temporal derivative. This allows individual neurons to advance their output firing rate with respect to their input.

Promisingly, prospective coding at the level of individual neurons has been observed experimentally. In the study by Köndgen et al., 2008, *in vitro* neurons are injected with a noisy sinusoidal current, and the average output is observed to be phase advanced for input frequencies on the order of 10 Hz. This average advance occurs at the level of short timescales, on the order of milliseconds. Additionally, recent experiments have also measured advanced responses on longer timescales, specifically in the case of neurons undergoing processes of threshold adaptation, such as e.g., spike frequency adaptation (Fuhrmann, Markram, and Tsodyks, 2002; Pozzorini et al., 2013) and more generally for adaptation processes with different time scales, like slow sodium-channel inactivation or after-hyperpolarization currents, involving power law dynamics (Lundstrom et al., 2008).

Taking inspiration from these experimental findings and theoretical insights, we perform a systematic study of prospective coding at the level of single neurons. We use different models for cortical neurons to explore the circumstances in which they can advance their output firing rate with respect to their input. Explaining the experimental findings by abstract computational models provides a mechanistic explanation for the biological phenomenon.

As a first contribution, we make use of experimental fits of neocortical and hippocampal neurons to the Hodgkin-Huxley model. By running numerical experiments, we show how the action potential generation mechanism allows to advance and delay signals, reproducing experimental findings. We show how these advances and delays can be observed for single neurons in single trials, rejecting the possibility that these prospective and retrospective responses are a mere statistical effect. One of the main advantages of using Hodgkin-Huxley equations to model neurons is that their parameters have clear mechanistic interpretations. Then, to elucidate the mechanisms behind prospectivity, we use simulation-based inference (SBI, Tejero-Cantero et al., 2020) to solve the inverse problem of finding what parameters of the model determine prospective responses in a neuron. Our analysis with SBI finds a reduced parameter space of three parameters that control prospectivity and retrospectivity, which allows us to hypothesize a mechanism for prospective firing, closely related to the speed of opening and closing of sodium channels.

As a second contribution, we present a simplified rate model for prospectivity, one that can reproduce the results stemming from Hodgkin-Huxley simulations at a fraction of the computational cost. We also extend this approach to more general rate models for which we show how adaptation processes can lead to prospective coding on much longer timescales, i.e., on the order of hundreds of milliseconds.

## 2 Results

### 2.1 Hodgkin-Huxley neurons can be prospective and retrospective

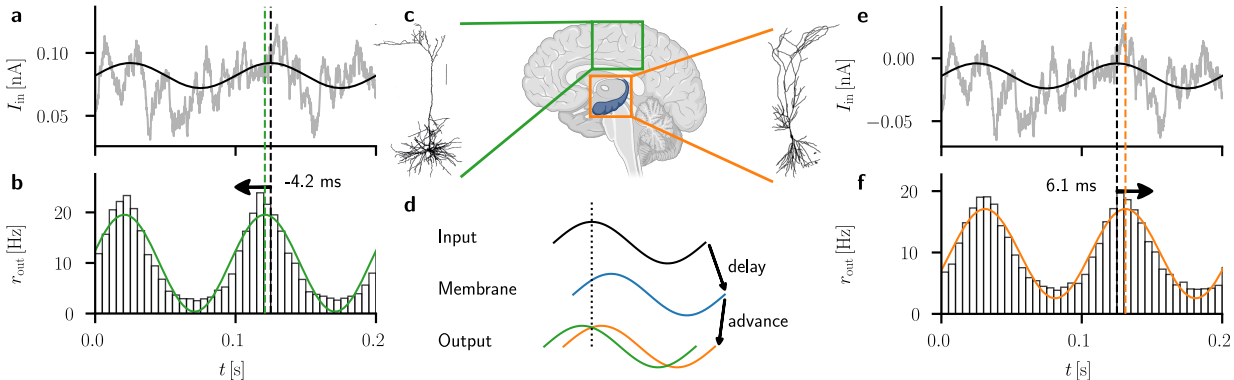


Figure 1: **Hodgkin-Huxley model parameters define whether neuronal firing is prospective or retrospective.** (a, b) The output firing rate  $r_{\text{out}}$  of a neocortical neuron model (Mainen et al., 1995) is phase-advanced by 4.2ms with respect to the 10Hz amplitude modulation of a noisy input current  $I_{\text{in}}$  (leftward arrow). The vertical dashed lines indicate the time of the maximum of the input modulation (black) and of the corresponding sinusoidal fit of the output rates  $r_{\text{out}}$  (green). Top: sample of  $I_{\text{in}}$  (grey). Bottom: averaged rate histogram. (c) Morphology of a neuron to which the parameters were fitted to and their corresponding brain regions (green: neocortex (Mainen et al., 1995), orange: hippocampus (Traub and Miles, 1991)). (d) While the membrane potential as a low-pass filtered input current is delayed with respect to the current, the output firing rate is advanced with respect to the voltage, overcompensating the delay (green, prospective with respect to the input) or not (orange, retrospective with respect to the input). (e, f) Analogously to (a, b), but for a hippocampal neuron (Brette et al., 2007), showing an average delay of 6.1 ms of the output rate with respect to the input modulation.

It has been reported that neurons can fire phase-advanced with respect to their input (Köndgen et al., 2008). We test whether we can reproduce this finding with typical Hodgkin-Huxley-type neuron models. To that end, we simulate Hodgkin-Huxley neurons with a sinusoidal 10 Hz input current with superimposed Ornstein-Uhlenbeck noise  $I_{\text{in}}$ . Indeed, we observe an advanced firing response (Fig. 1a-b) with parameters fitted to cortical pyramidal neurons (Fig. 1c, green). The shift of 4.2ms is in accordance with findings of *in vitro* experiments with cortical neurons (Köndgen et al., 2008). If we repeat the simulation with parameters fitted to hippocampal neurons, (Fig. 1c, orange), we observe that the firing response of the neuron to sinusoidal input is delayed by 6.1 ms (Fig. 1e-f). Thus, Hodgkin-Huxley neurons can show both advanced and delayed firing for input modulated with the same frequency.

The process of integrating the input current into the membrane voltage  $V_m$  naturally introduces a delay with respect to  $I_{\text{in}}$ . As the output rate  $r_{\text{out}}$  depends on the membrane voltage, one would intuitively expect the output rate to also be delayed—but previous experimental results observe that this is not necessarily the case (Linaro, Biró, and Giugliano, 2018). That  $r_{\text{out}}$  can be advanced with respect to  $I_{\text{in}}$  supports the hypothesis that individual neurons can implement prospective coding. For this, there must be some mechanism that compensates for the delay introduced by the membrane filtering. The proportion between the delay from input to membrane and the advance from membrane to output defines whether a given neuron is in the prospective or retrospective regime (Fig. 1d).

Interestingly, we observe that the parameters of the Hodgkin-Huxley model influence whether the output of a neuron is prospective or retrospective with respect to the input. This indicates that we can change the temporal response of such a neuron by changing a certain subset of relevant parameters. Finding these relevant parameters for the Hodgkin-Huxley model, parameters which are derived from well-known biological mechanisms, allows us to propose a biologically plausible mechanistic explanation for prospective coding in individual neurons.

## 2.2 A mechanism for prospective coding in Hodgkin-Huxley neurons

**SBI and relevant parameters** To investigate the mechanisms by which neurons can advance or delay their output with respect to their input, we perform a phase space analysis of the Hodgkin-Huxley model, sampling its parameters by means of SBI (see Tejero-Cantero et al., 2020, and also Methods). We use SBI to determine which Hodgkin-Huxley parameters strongly influence the temporal response of the neuron. We start with a set of 9 parameters,  $\theta$ , relevant for the spiking mechanism of the Hodgkin-Huxley model. These are the leakage conductance  $g_\ell$ , the sodium and potassium conductance  $\bar{g}_{\text{Na}}$  and  $\bar{g}_{\text{K}}$  and the opening and closing variables of the ion channel gating particles  $\alpha_m$ ,  $\beta_m$ ,  $\alpha_h$ ,  $\beta_h$ ,  $\alpha_n$  and  $\beta_n$  (see Fig. SI.2 in SI). To discern which among these parameters are important for distinguishing prospective and retrospective firing, we compare the posterior distribution  $p(\theta|x)$ , conditioned on temporal phase shifts  $x$ . We estimate these posteriors with SBI, assuming Gaussian prior distributions  $p(\theta)$  centered at the cortical parameters (see Methods).

The parameters that influence the temporal response should have narrow posterior distributions that do not overlap for the different observation. According to this criterion, we determined that the relevant parameters are  $g_\ell$ , which influences the membrane time constant of the neuron,  $\alpha_m$ , corresponding to the opening of the sodium ion channels and hence the action potential initiation, and  $\beta_h$ , which controls the closing of the sodium ion channels. See Methods for a more detailed discussion.

**Posterior analysis** To go further, we reduce our sampling to these three parameters, while keeping the others constant and equal to those measured in neocortical neurons (Fig. 2). To verify whether the reduced model is able to yield diverse advances and delays, we perform simulations with parameters drawn from a posterior that is conditioned on different phase shifts. We condition the posterior on an advance (−10 ms), instantaneous firing (0 ms) and a delay (10 ms). Running simulations with parameters sampled from each conditional posterior yields distributions of phase shifts that are centered around the corresponding time shifts (Fig. 2j). This shows that the model is capable of producing a variety of advances and delays and that the inference of the posterior leads to meaningful distributions. The distribution of phase shifts is narrow for the advanced condition and becomes wider from instantaneous to delayed firing, indicating a stronger sensitivity to small fluctuations of the parameters the further we move away from the original neocortical parameters (that show advanced firing). A typical set of parameters for each posterior condition is shown in Fig. 2a-i, together with an example of the noisy input trace using the same noise realization in all three cases. The shift of the average firing rate  $r_{\text{out}}$  indeed reproduces the phase shift that we use as condition for the posterior (Fig. 2d-f). Interestingly, the shift of the temporal response can also be observed for spikes in single neurons (Fig. 2g-i). This is an important observation as the shift of  $r_{\text{out}}$ , the measurement of which needs many repeated trials or neurons, is clearly visible even at the level of the output of a single neuron in a single trial. This is a clear indication that prospective coding in these neurons cannot be cast aside as a purely statistical effect.

**Mechanistic explanation** The opening and closing rates  $\alpha_m$  and  $\beta_h$  can be combined to define the more intuitively comprehensible time constants  $\tau_m = 1/(\lambda_{\alpha_m}\alpha_m + \beta_m)$  and  $\tau_h = 1/(\alpha_h + \lambda_{\beta_h}\beta_h)$  (Fig. 2b-c) and steady states  $m_\infty = \lambda_{\alpha_m}\alpha_m/(\lambda_{\alpha_m}\alpha_m + \beta_m)$  and  $h_\infty = \alpha_h/(\alpha_h + \lambda_{\beta_h}\beta_h)$  of the gating variables (Fig. 2d-e). Using these parameters, it is easy to visualize an underlying mechanism for prospectivity in Hodgkin-Huxley neuron. For the advanced condition, both time constants are smaller as compared to the instantaneous and delayed conditions. This leads to a faster activation and deactivation of the sodium channels. Additionally, both steady states are shifted slightly to the left in the advanced condition, indicating an earlier opening of the  $m$ -gates and an earlier closing of the  $h$ -gates for a rising  $V_m$ —as during an action potential initiation. Because the activation and inactivation of the sodium channels is shifted earlier in time and happens faster, the peak of the sodium conductance, and with it the peak of the action potential, occurs earlier in time with these parameters. Because the action potential happens earlier in time, the output rate of the neuron is advanced too, a mechanism that is supported by the voltage traces shown in Fig. 2g-i. Additionally,  $g_\ell$  influences the membrane time constant and a larger  $g_\ell$  leads to a faster integration of input.

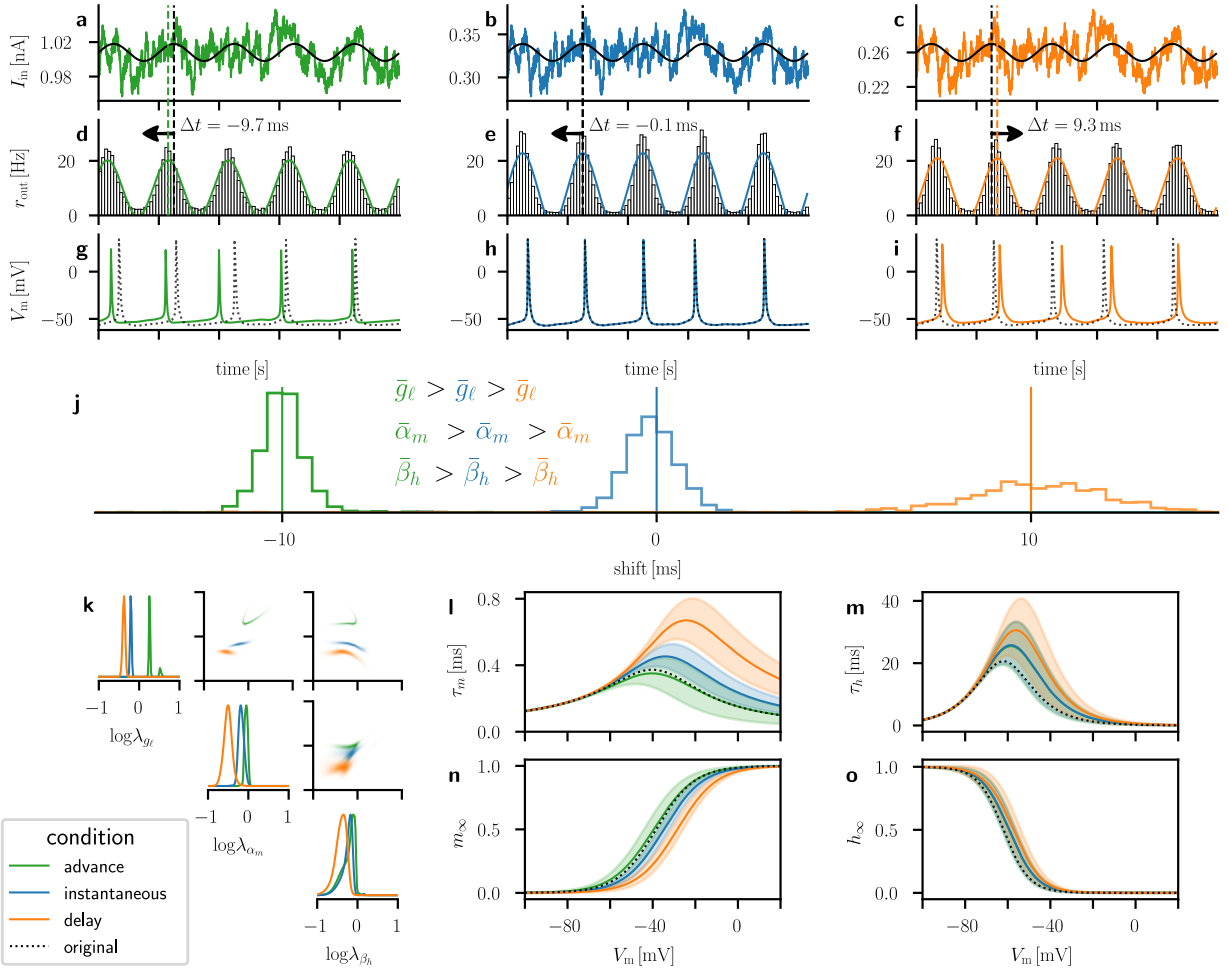


Figure 2: **Examples of prospective (green), instantaneous (blue) and retrospective (orange) firing of a Hodgkin-Huxley neuron with different parameters.** (a-i) Identical noisy input currents (a-c) that are sinusoidally modulated (black) produce an averaged firing rate that is advanced (d), instantaneous (e), or delayed (f) for different parameters  $\alpha_m$ ,  $\beta_h$  and  $g_\ell$  of the sodium activation, inactivation and the leak conductance. (g-i): Voltage traces to the identical current sample shown above (dotted line identical to the middle trace for reference). (j) The distribution of phase shifts, calculated from the input current to the output rate, as shown in (a-f), with parameters drawn from the posterior distribution conditioned on prospective ( $-10$  ms, green), instantaneous 0 (blue) and retrospective (10 ms, orange) firing. (k) The posterior densities of the parameters  $g_\ell$ ,  $\alpha_m$  and  $\beta_h$ , conditioned on a phase shift being advanced (green), 0 (blue) or delayed (orange) as in j, while fixing the remaining parameters. Abscissa representing the logarithm of the factor  $\lambda_\theta$  that scales the corresponding parameter  $\theta$ . The three diagonal plots show the conditional posterior densities of a single parameter, with the other two parameters fixed to the maximum of the joint density. The 2-dimensional plots show the densities of the parameter to the left and below, with the third parameter fixed. (l – o) Time constants and steady states of the gating variables  $m$  and  $h$  as a function of the voltage, with standard obtained from sampling the joint parameter density conditioned on advanced (green), 0 (blue) and delayed (orange) phase shifts. Black dotted line refers to the original parameters of the cortical neuron (Mainen et al., 1995).

### 2.3 Advanced and delayed spike responses to stationary stochastic inputs

Although these are very interesting results, the advance and delay with respect to periodic sinusoidal signals might seem to be a simple task, and not so expressive of robust predictive coding in these neurons. There-

fore, we next compare the temporal response of different neurons receiving input without any sinusoidal modulation. To make a statement about the advance or delay of a neuron’s response to some input we need a reference signal—usually the input. While for sinusoidal input the advance can be estimated by the phase of a sinusoidal fit of the output rate, for random-like signals we can consider the cross-correlation between the output of networks with different parameters to the same input as estimation. Thus, to compare the temporal shift of a prospective neuron to that of a retrospective neuron we simulate a single neuron with parameters from the advanced, instantaneous and delayed condition as shown in Fig. 2, that receives input without any amplitude modulation and superimposed noise only, that is the same for each neuron, as shown in Fig. 3a. The instantaneous neuron is used as a reference and the temporal shift of the other two neurons is estimated by cross-correlation. The spikes of the neuron with parameters from the advanced condition are advanced by approximately 7ms compared to the instantaneous neuron. Similarly, the neuron with parameters from the delayed condition is delayed by 8ms.

Although the advance in the response of the neurons to noise estimated from the cross-correlation is smaller than the average advance of the response to sinusoidal modulated input estimated by sinusoidal fits, the results reflect a consistent advance and delay relative to a reference signal. It is reassuring to find that prospectivity and retrospectivity are consistent across the comparison between a sinusoidal input and this case of inputs consisting of pure noise. Nonetheless, it is important to test whether this extends to more informative signals that include modulation. In order to account for this, we investigate the temporal response of Hodgkin-Huxley neurons to more complex signals.

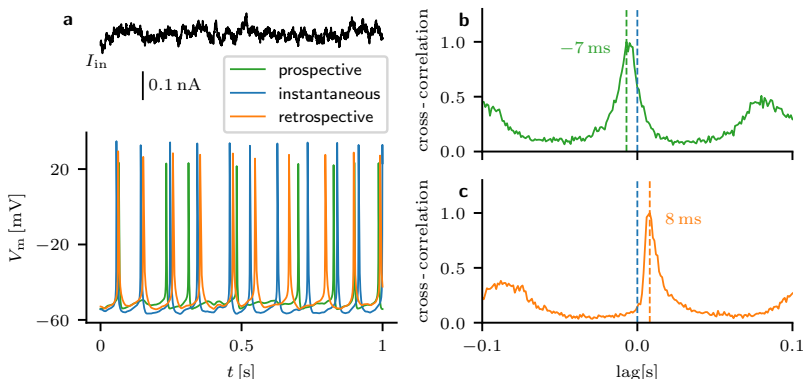


Figure 3: **Advanced and delayed spiking to the same stationary input current.** (a) Voltage response to a stationary noisy current (black) for the 3 sets of parameters used in Figure 1. The mean of the input is adapted to achieve the same average firing rates. (b, c) Spike cross-correlogram for the prospective (b) and the retrospective (c) neuron parameters, with the spike times of instantaneous parameter set as reference. The spikes of the prospective neuron are on average advanced by 7 ms, and that of the retrospective neuron on average delayed by 8 ms, compared to the spikes of instantaneous neuron. The secondary peaks left and right correspond to the average inter-spike interval of 0.1 s. The statistics is based on a total simulation length of 100 s.

## 2.4 The phase-advance is robust to a wide range of inputs

Compared to the complex input dynamics a biological neuron encounters *in vivo*, predicting a sinusoidal seems like an easy task. Even though we add high amplitude noise, the input spectrum is dominated by the sine frequency. Input signals of biological neurons, though, can be random-like and often contain informative signals with a non-trivial frequency spectrum. The response of a neuron depends on the input frequency (Hutcheon and Yarom, 2000). In particular, the presence of a phase advance in the response strongly depends on the input signal frequency. In this section, we investigate the response of a Hodgkin-Huxley neuron to inputs with different frequencies. Further on, we show that these neurons can also be prospective with respect to random-like input.

As observed experimentally, for the cortical parameters we observe a peak of the amplitude of  $r_{out}$  that indicates a resonance frequency of the neuron to specific input as well as an advance of  $r_{out}$  with respect to

$I_{in}$  only for lower frequencies (Fig. 4a-b). It is well-known that Hodgkin-Huxley can reproduce this resonator behavior (REF). Thus, we expect no prospectivity for high frequencies and a distorted firing response for signals that include frequencies close to the resonance frequency. To show that prospective coding can be observed for random-like signals, we use a superposition of sinusoidals with a combination of random frequencies.

We simulate three different random-like signals  $I_{in}$  to which we add Ornstein-Uhlenbeck noise to obtain the firing response  $r_{out}$  (Fig. 4c-e). The first signal contains smaller frequencies that lead to changes on a large time scale and shows a clear phase advance (Fig. 4c). For the second signal, we considered higher frequencies such that  $r_{out}$  is slightly skewed but still shows an advance of  $r_{out}$  with respect to  $I_{in}$  (Fig. 4d). To illustrate the effect of the resonance frequency, we added a component to the first signal with a small amplitude and frequency of 11 Hz, that is barely visible in  $I_{in}$  but very prominent in  $r_{out}$  (Fig. 4e). For all three signals, the cross-correlation between  $r_{out}$  and  $I_{in}$  is maximal at approximately  $-25$  ms (Fig. 4f-h) matching the phase delay one would expect from the phase response shown in Fig. 4b. Considering the same inputs to neurons with the hippocampal parameters, we observe a similar response, but with an advance of around 7 ms, as expected from the frequency response shown in Fig. 4a and b. While we do see prospective firing for these neurons, contrary to their response to a 10 Hz sinusoidal input, the advance is much smaller as compared to the neo-cortex neurons.

These results show that neurons can perform prospective firing also in the case of random-like input. The exact phase and amplitude of the response, though, highly depend on the exact frequencies that characterize the signal.

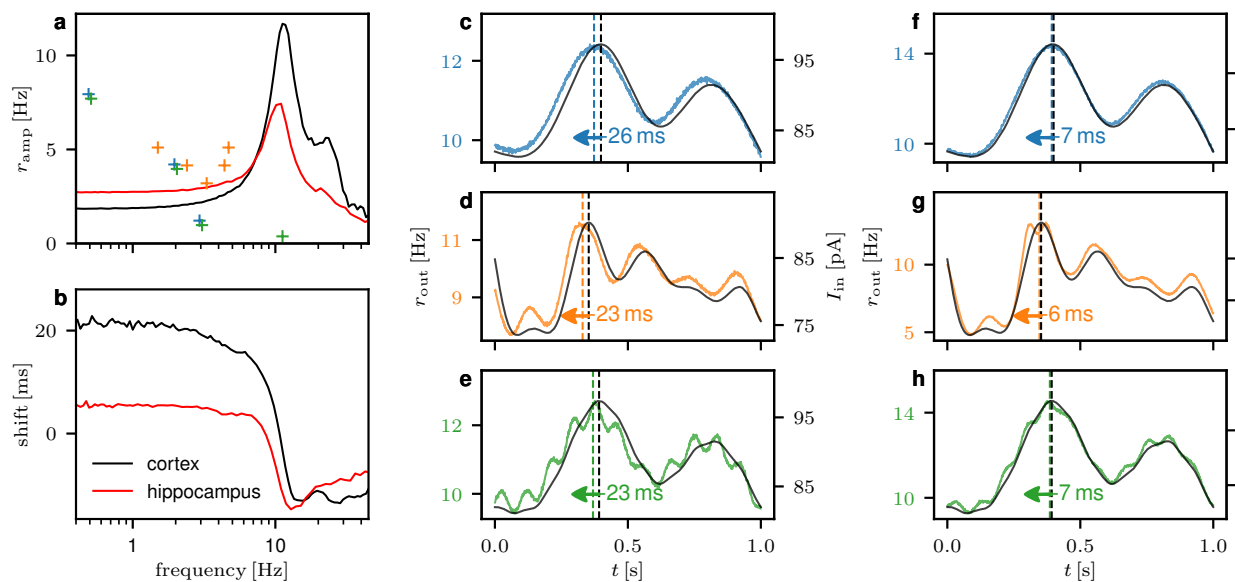


**Figure 4: The temporal advance is robust to wide range of time-varying inputs.** (a) The amplitude response of a Hodgkin-Huxley neuron to sinusoidal input is frequency dependent and shows a resonance frequency at 11 Hz for the cortical parameters (black) and slightly less for the hippocampal parameters (red). Colored crosses indicate the frequency and amplitude of the Fourier components composing the mean input currents in c-h. (b) Phase as a function of the frequency, showing an advance of  $r_{out}$  for frequencies  $\leq 11$  Hz (cortical parameters) and  $< 10$  Hz for the (hippocampal parameters), and a delay for higher frequencies. (c-e) Averaged firing rates (colored) of the cortical neuron to the randomly modulated noisy input currents combining the Fourier components indicated in a) (average current in black). Dashed lines with arrows indicate the phase-advance computed from the cross-correlation between average current and rate. (c) With low frequency components,  $r_{out}$  is largely advanced with respect to  $I_{in}$ . (d) Including higher frequencies still shows an advance, although more skewed. (e) Adding an additional resonance frequency at 11 Hz to the signal in (c), time-advanced oscillations emerge in  $r_{out}$ . (f-h) Same as in c-e, but for the hippocampal neuron, showing only a modest advance.

## 2.5 Adaptation processes and prospective coding

We next show that prospective coding can be derived analytically from an approximation of Hodgkin-Huxley dynamics. To do this, we consider slow voltage dynamics (i.e. low frequencies) with small fluctuations (i.e., small amplitudes). The approximation shows that such prospective dynamics can be developed for different kinds of adaptation processes taking place on different time scales. For this generalization, the main example we use is threshold adaptation.

**Hodgkin-Huxley adaptation** We introduce a simplified Hodgkin-Huxley model for which we assume the output rate of a neuron to be a function of the sodium conductance  $r = \varphi(g_{\text{Na}}) = \varphi(m^3h)$ , with sodium activation variable  $m$  and inactivation variable  $h$ . Since the activation is fast, we approximate  $m$  to be an instantaneous function of the voltage,  $m \approx m_\infty(v)$ . We approximate the dynamic inactivation variable  $h$  by  $h = h_\infty(v) - \tau_h(v)\dot{h} \approx h_\infty(v) - \tau_h(v)\dot{h}_\infty(v)$ , where we replaced  $\dot{h} \approx \dot{h}_\infty = h'_\infty \dot{v}$ . This leads to the approximation of the sodium conductance,

$$g_{\text{Na}} = m^3h \approx m_\infty^3(v)(h_\infty(v) - \tau_h(v)h'_\infty(v)\dot{v}) = g_{\text{Na}}^\infty(v) + \tau_r^{\text{HH}}(v)g_{\text{Na}}^{\infty\prime}(v)\dot{v} = g_{\text{Na}}^\infty(v) + \tau_r^{\text{HH}}(v)\dot{g}_{\text{Na}}^\infty \quad (1)$$

where  $g_{\text{Na}}^\infty = m_\infty^3h_\infty$  is the steady state and  $\tau_r^{\text{HH}} = -\frac{\tau_h m_\infty^3 h'_\infty}{g_{\text{Na}}^{\infty\prime}}$  the effective time constant of the sodium conductance, both functions of  $v$ . Since this time constant is positive, Eq. (1) describes a prospective mechanism on the level of the sodium conductance. Indeed, because  $h'_\infty$  is always negative,  $\tau_r^{\text{HH}}$  is positive as long as  $g_{\text{Na}}^{\infty\prime}(v)$  is positive. Considering the Hodgkin-Huxley parameters fitted to cortical neurons,  $g_{\text{Na}}^{\infty\prime}(v)$  is in fact positive for voltages below  $-40$  mV and for any fluctuations close to the leakage voltage that is  $-65$  mV.

To express the output rate of a neuron in terms of the prospective voltage, we move the temporal dynamics into the sodium steady state and Taylor expand for small voltage fluctuations  $\dot{v}$  such that we get for the right-hand side of Eq. (1) the approximation  $g_{\text{Na}}^\infty(v) + \tau_r^{\text{HH}}g_{\text{Na}}^{\infty\prime}(v)\dot{v} \approx g_{\text{Na}}^\infty(v + \tau_r^{\text{HH}}\dot{v})$ . With this, we rewrite the estimate of the output rate in our model as

$$r_{\text{HH}} = \varphi(g_{\text{Na}}) \approx \varphi(g_{\text{Na}}^\infty(v + \tau_r^{\text{HH}}\dot{v})) = \varphi_{\text{HH}}(v + \tau_r^{\text{HH}}\dot{v}) = r_{\text{HH}}^{\text{pros}}. \quad (2)$$

Here,  $r_{\text{HH}}$  refers to the full dynamics of  $g_{\text{Na}} = m^3h$  with no approximations and  $r_{\text{HH}}^{\text{pros}}$  is our approximated model that based on the prospective voltage  $v + \tau_r^{\text{HH}}\dot{v}$ . In this approximation, the dynamics of  $g_{\text{Na}}$  is absorbed in the function  $\varphi_{\text{HH}}$  of the voltage, while the effect of the adaptation of  $h$  is expressed by the term  $\tau_r^{\text{HH}}\dot{v}$ .

Because  $r_{\text{HH}}^{\text{pros}}$  is a function of the prospective voltage, its time course will be advanced with respect to the original voltage. The prediction of our model is that also  $r_{\text{HH}}$ , and hence also  $g_{\text{Na}}$ , are advanced. Naturally,  $r_{\text{HH}}^{\text{pros}}$  and  $r_{\text{HH}}$  should not diverge too much for the approximations to be accounted valid. If either  $\tau_h$  or  $\dot{v}$  are large, the approximations for  $h$  becomes worse.

To verify the model, we simulate a random-like membrane voltage, as in Section 2.4, which is shown in Fig. 5a. We can see that  $r_{\text{HH}}^{\text{pros}}$  approximates  $r_{\text{HH}}$  well with small deviations for high rates. Most importantly, both rates show a similar advance compared to the instantaneous rate  $r_{\text{HH}}^\infty = \varphi_{\text{HH}}(v)$ . We use the instantaneous rate instead of just the voltage  $v$ , as the nonlinear activation function shown in Fig. 5b leads to skewed rates and makes a direct comparison impractical. In Fig. 5b, we show how  $r_{\text{HH}}$  evolves for different  $v$  as compared to the steady state  $r_{\text{HH}}^\infty$ . The circular shifts around the nonlinear rate function indicate a temporal shift between the two variables. While the temporal direction is not shown explicitly, a clockwise rotation corresponds to an advance and a counter-clockwise rotation to a delay.

Finally, we verify our prediction that the approximations in our model lead to divergences between  $r_{\text{HH}}^{\text{pros}}$  and  $r_{\text{HH}}$  if either  $\tau_h$  or  $\dot{v}$  are large by increasing the frequency of a sinusoidal input and thus increasing  $\dot{v}$ . In Fig. 5c, we show that the estimation of the temporal shift based on  $r_{\text{HH}}^{\text{pros}}$  approximates the shift estimated with  $r_{\text{HH}}$  well for small frequencies. If we increase the frequency, the two estimations diverge until they both reach zero again for high frequencies. Notably, both models replicate the decrease in temporal shift for increasing frequency that we showed for the spiking Hodgkin-Huxley model in Fig. 4b.

The adaptation process described so far replicates the prospective aspect of the spiking Hodgkin-Huxley model while constituting a much simpler model. Including the input current, and with it the integration delay



by the membrane time constant  $\tau_m$ , the model can be extended to incorporate retrospective coding when comparing the output rate to the input current and adapting  $\tau_m$  accordingly. Still, with this model, we are limited to small time scales, and it does not correctly describe, as is, prospectivity at longer timescales. To show that prospective coding is a more general principle that can be achieved through multiple mechanisms, we introduce a similar but more general threshold adaptation model.

**Threshold adaptation** To give an intuition of why adaptation leads to a prospective firing, we write the firing rate as  $r = \psi(v - \vartheta) = \psi(v_\vartheta)$ , where  $v_\vartheta$  describes the distance of the voltage to the threshold. The threshold dynamics is such that  $\vartheta$  slowly increases when the voltage increases. Specifically, the threshold dynamics is given by

$$\dot{\vartheta} = \frac{\vartheta_\infty(v) - \vartheta}{\tau_\vartheta(v)} \quad (3)$$

where the steady state of the threshold  $\vartheta_\infty(v)$  is a monotonically increasing function of the voltage (typically a sigmoidal akin to  $m_\infty(v)$ ), and  $\tau_\vartheta(v)$  is bell-shaped (in analogy of  $\tau_m$  above, but with timescales on the order of 100 ms up to 1 s, see Methods). Analogously, as we approximated  $h$  above, we now approximate  $\vartheta = \vartheta_\infty(v) - \tau_\vartheta(v) \dot{\vartheta} \approx \vartheta_\infty(v) - \tau_\vartheta(v) \vartheta'_\infty(v) \dot{v}$ . Using this approximation we write the distance to the threshold as

$$v_\vartheta = v - \vartheta \approx v - \vartheta_\infty(v) + \tau_\vartheta(v) \vartheta'_\infty(v) \dot{v} = v_\vartheta^\infty(v) + \tau_r^\vartheta(v) v_\vartheta^{\infty'}(v) \dot{v} = v_\vartheta^\infty(v) + \tau_r^\vartheta \dot{v}_\vartheta^\infty(v) \quad (4)$$

with the steady state of the distance between voltage and threshold  $v_\vartheta^\infty(v) = v - \vartheta_\infty(v)$  and  $\tau_r^\vartheta = \frac{\tau_\vartheta(v) \vartheta'_\infty(v)}{v_\vartheta^{\infty'}(v)}$  estimating the time constant of the prospective mechanism described by the right-hand side of Eq. (4).

As in the derivation for the prospective firing based on sodium inactivation, we Taylor expand the steady-state function for small variations  $\dot{v}$  as  $v_\vartheta^\infty(v) + \tau_r^\vartheta(v) \dot{v} \approx v_\vartheta^\infty(v) + \tau_r^\vartheta(v) v_\vartheta^{\infty'}(v) \dot{v}$ . Inserting this approximation into Eq. (4), we rewrite the estimate of the output rate

$$r_\vartheta = \psi(v - \vartheta) \approx \psi(v_\vartheta^\infty(v) + \tau_r^\vartheta \dot{v}) = \psi_\vartheta(v + \tau_r^\vartheta \dot{v}) = r_\vartheta^{\text{pros}}, \quad (5)$$

which implicitly defines the transfer function  $\psi_\vartheta$ . As for the Hodgkin-Huxley adaptation, the dynamics of the threshold adaptation is absorbed in the function  $\psi_\vartheta$  of the voltage, while the effect of the changing threshold is expressed in the term  $\tau_r^\vartheta \dot{v}$ . Keeping the notation similar, we refer to the original rate as  $r_\vartheta$ , while  $r_\vartheta^{\text{pros}}$  is the approximated rate based on the prospective voltage  $v + \tau_r^\vartheta \dot{v}$ .

Fig. 5d shows that both the rate function  $r_\vartheta$  with the dynamic threshold and the prospective rate  $r_\vartheta^{\text{pros}}$ , yield a firing rate that is advanced to the instantaneous rate in the order of  $\tau_r^\vartheta(v)$  in response to the variable input. Note that the time scale is larger by a factor of 10 as compared to the Hodgkin-Huxley adaptation. Again, we compare the output rate to the instantaneous steady-state rate  $r_\vartheta^\infty(v) = \psi_\vartheta(v)$ , shown in Fig. 5e, to account for the non-linearity of the transfer function. Similar to the Hodgkin-Huxley adaptation, we observe an advance, but this time in the order of 100 ms.

Because the threshold adaptation is a more general mechanism and works on different time scales, we are free to choose the relevant time constants. In this case, we set  $\tau_r^\vartheta(v_0)$  to 100 ms for the mean voltage  $v_0 = -60$  mV, which corresponds to the maximal temporal shift for small variations of low frequencies around  $v_0$ , considering prospective dynamics in the form of  $v + \tau_r \dot{v}$ . For higher frequencies, the shift will decrease as shown in Fig. 5f. Comparable to the Hodgkin-Huxley adaptation, the shift of the rate with threshold dynamics and our approximated prospective rate will diverge for increasing frequencies because we progressively violate our assumption of slow fluctuations. But, qualitatively the two shifts show the same features, starting with a shift of 100 ms for low frequencies and decreasing for higher frequencies towards zero.

**Active dendrites and prospective coding** Sinusoidal stimulation of apical dendrites *in vitro* can lead to an advanced voltage response in the soma of cortical pyramidal neurons (Ulrich 2002, Dendritic resonance in rat neocortical pyramidal cells). The advanced response is assigned to the dendritic  $I_h$  current that slowly counteracts voltage de- and hyper-polarizations in the apical dendrite. The somatic impact of the dendritic  $I_h$  could be described in a 1-compartment model in analogous terms as we described threshold adaptation.

Instead of subtracting a threshold that slowly increases with the voltage,  $r = \psi(v - \vartheta)$ , one may add an  $I_h$  current that slowly decreases with the voltage,  $r = \psi(v + I_h)$ , leading similarly to a temporally advanced response.

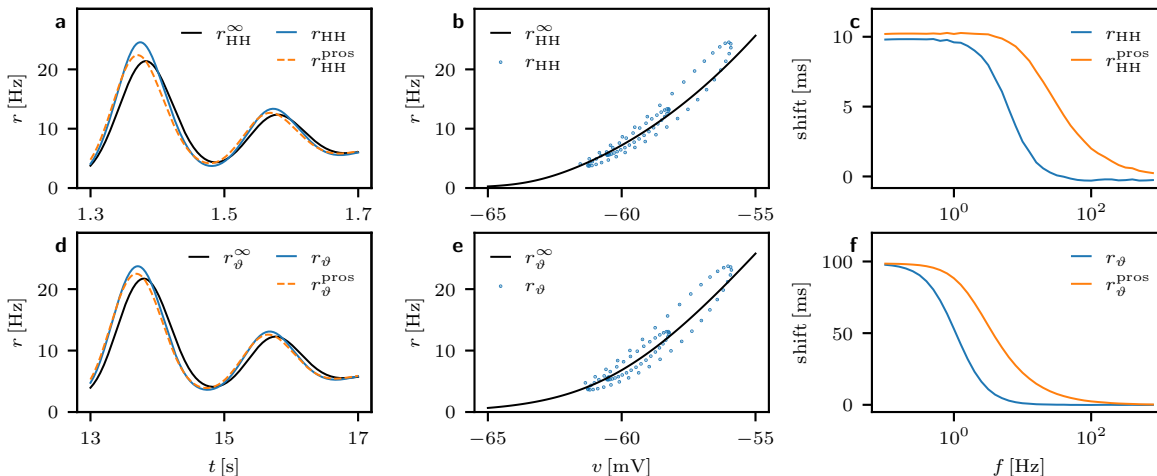


Figure 5: **A fast spike- and slow threshold-adaption lead to temporal advances on different time scales.** (a) The output rate of a neuron as a function of the sodium conductance  $r_{\text{HH}} = \varphi(g_{\text{Na}})$  (blue) is prospective with respect to the instantaneous rate  $r_{\text{HH}}^{\infty}(v) = \varphi(g_{\text{Na}}^{\infty}(v))$  (black). The approximated rate  $r_{\text{HH}}^{\text{pros}}$  matches  $r_{\text{HH}}$  well and shows a similar advance (dashed orange). (b) Firing rates  $r_{\text{HH}}$ , sampled every 50 ms (blue dots), turn clockwise around the steady-state voltage-to-rate transfer function ( $r_{\text{HH}}^{\infty}(v)$ , black). (c) Time-advance of  $r_{\text{HH}}$  (blue) and the approximation  $r_{\text{HH}}^{\text{pros}}$  (orange) with respect to the voltage for different frequencies. The approximation qualitatively reproduces the advance that decays with increasing frequencies. (d-f) Corresponding rate functions for the threshold adaptation model, with  $r_{\vartheta} = \psi(v - \vartheta)$  (blue) and a dynamic threshold  $\vartheta$  being the original model,  $r_{\vartheta}^{\text{pros}} = \psi_{\vartheta}(v + \tau_r^{\vartheta} \dot{v})$  (dashed orange) its approximation, and the instantaneous rate  $r_{\vartheta}^{\infty}(v) = \psi_{\vartheta}(v)$  (black), in analogy to the sodium inactivation in (a-c). The 10 times longer time scale (d, as compared to a) reflects the slower modulation of the input in the threshold adaptation model, resulting in a 10 times larger time-advance (f, 50 ms) as compared to sodium inactivation model (c, 5 ms).

### 3 Discussion

**Summary** Wielding the power of both statistical analysis and simplified models, our results show how neurons of the cortex can be prospective with respect to their input. Prospectivity is widely expected to happen in the brain at the population level, but here we show how it can already manifest at the level of individual neurons. In this work (i) we find that the Hodgkin-Huxley model can reproduce experimental *in vitro* results regarding prospective and retrospective behavior in cortical neurons. (ii) By studying the parameter space of Hodgkin-Huxley neurons around the cortical parameters we can characterize a general mechanism behind prospectivity at timescales of tens of milliseconds. (iii) We developed a simplified and general model for prospectivity that is compatible with these results, while minimizing complexity. (iv) Our models all show that adaptation translates into a temporal advance by a push-pull mechanism.

To provide a rough intuition for the time advance, consider a rate that is growing and returning back after the peak. Adaptation effectively pushes this rate back earlier. After returning to a low rate and recovery from the adaptation, the rate may start growing again. During this, recovery effectively pulls the rate up earlier as compared to the non-recovered state. Overall, the early pushing down and early pulling up leads to a temporal advance on the time scale of the adaptation process. We considered adaption of the sodium inactivation on the time scale of 10 ms, and threshold adaptation on the time scale of 100's of ms. But other types of adaptation, for instance caused by dendritic  $I_h$  currents, may further contribute to prospective coding (Senn et al., 2024).

**Related work** Our results replicate experimental findings showing that individual neurons can be prospective on a variety of timescales. At the timescales of several milliseconds, various works (Köndgen et al., 2008; Lundstrom et al., 2008; Ostojic et al., 2015; Linaro, Biró, and Giugliano, 2018) have shown that neurons can be prospective for noisy periodical inputs. These works were an inspiration to our models. Fuhrmann, Markram, and Tsodyks (2002) and Pozzorini et al. (2013) explicitly showed how—at longer timescales—spike frequency adaptation also leads to a prospective output at the level of individual neurons. Moreover, recent theoretical work has leveraged the existence of neuron-level prospectivity to propose general frameworks for computation and learning in the brain and in bio-inspired hardware NLA, LE, GLE. Our theoretical work connects these diverse findings into an overarching coherent picture.

**Hodgkin-Huxley and prospectivity** We used existing parameter fits of the model to neocortical and hippocampal neurons to show that we can reproduce experimental results on phase advance and delay respectively, when these neurons are injected with noisy periodical signals. Notably, modifying the Hodgkin-Huxley parameters can change these phase advances into phase delays, or delays into advances. This makes the Hodgkin-Huxley model a good starting point to explore the underlying mechanisms behind this temporal processing. More specifically, this flexibility of Hodgkin-Huxley allows us to narrow down the parameter space to a reduced set of relevant parameters, pointing to a specific mechanistic explanation of prospectivity and retrospectivity at these timescales. Evolutionarily speaking, it makes sense that neurons can exhibit a range of advances and delays.

Simulation-based inference allows us to perform this model reduction in a systematic and rigorous way. We could mark down three parameters as those most involved with temporal processing:  $g_\ell$ ,  $\alpha_m$ ,  $\beta_h$ , with time advances increasing for increased values of all these parameters. This suggests a simple mechanism for prospectivity, where a faster activation and deactivation of the sodium channels leads to earlier spiking, and eventually to prospective spiking. This mechanism accounts for temporal shifts on the order of the time constants involved, which can more than compensate for the delays related to membrane integration. We also show that the relative advance and delay can be observed even in the absence of any sinusoidal modulation of the input, and appears for individual neurons and not only statistically. Specifically, by using the spike times of the instantaneous neuron as a temporal reference, we find that prospective and retrospective coding can be observed on the level of single neurons and single spikes, and is therefore not a statistical effect of average outputs.

Importantly, prospectivity and retrospectivity seem to depend on the frequency of the input. For the sinusoidal-like input we use for SBI, lower frequencies favor prospectivity, whereas higher frequencies elicit retrospective responses. By combining a randomized set of frequencies we emulated a random-like input that might be seen as more biologically plausible. We systematically find prospectivity for cortical neurons in cases where the dominant frequencies are not higher than  $\sim 10$  Hz.

**Generalization** From a wider perspective, prospectivity is known to occur at different timescales, notably through the mechanism of spike frequency adaptation (Pozzorini et al., 2013), which goes beyond the scope of the Hodgkin-Huxley model. Inspired by this, we proposed and tested a generic shape for the voltage dependency within neuronal activation functions. We propose approximations that make explicit a sensitivity of the output to the rate of change of the voltage  $\dot{v}$ . This represents a general recipe for a model-agnostic description of prospectivity at the neuronal level. This has the advantage of applying to any characteristic timescale  $\tau_r$  of the prospective mechanism. Within the limitations of such a simplified universal description, we find good agreement with prospective timescales in Hodgkin-Huxley and spike frequency adaptation, using synthetic inputs that emulate typical biological signals. Our models are simple but powerful enough to describe processes occurring at different timescales, and also at combinations of several timescales. This universal approach can thus serve as a first step in explaining prospectivity and retrospectivity in cortical neurons, and links biology and recent abstract models of prospectivity in the brain.

**Conclusions** To conclude, this work shows how prospectivity at the level of individual neurons is not only plausible as shown by experiments, but also realizable in terms of different mechanisms. The work contributes to a better theoretical comprehension of these mechanisms, which ultimately could be related to the capabilities of brains in terms of both prospective learning and retrospective memory storage. Fi-

nally, the work provides justifications and biological plausibility to theoretical models that include simplified prospective mechanisms at the level of individual neurons.

## 4 Methods

### 4.1 Hodgkin-Huxley model

The Hodgkin-Huxley model (Hodgkin and Huxley, 1952) remains one of the most important representations of action potential generation in neurons. It incorporates the voltage-gated sodium and potassium channels, which are modeled by four gating particles each. A sodium channel consists of three  $m$  and one  $h$  gating particles, while the potassium channel consists of four  $n$  gating particles. A single channel is only open for ion transmission if all four gating particles are in an open configuration. The variables  $m$ ,  $h$  and  $n$  each describe the fraction of corresponding gating particles in the open configuration. The total conductance of a channel is usually modeled by the maximal conductance (e.g.  $\bar{g}_{Na}$ ) times the fraction of open channels which is defined by the fraction of gating particles in the open conformation (e.g.  $g_{Na} = \bar{g}_{Na}m^3h$ ).

During the initial phase of the action potential and the rising phase of the membrane potential  $V_m$ , the fast opening of the sodium channels through the  $m$  gates leads to an increased influx of sodium ions which leads to a steep increase in  $V_m$  (depolarization). The subsequent closing of the  $h$  gates leads to a closing of the sodium channels and stops the influx of sodium ion. Meanwhile, the potassium channels open through the slow opening  $n$  gating particles and the efflux of potassium ions leads to a repolarization and hyperpolarization of  $V_m$  in the late phase of the action potential.

Mathematically, the Hodgkin-Huxley model can be described by the dynamics of the membrane potential  $V_m$ :

$$C_m \dot{V}_m = g_\ell(E_\ell - V_m) + \bar{g}_{Na}m^3h(E_{Na} - V_m) + \bar{g}_K n^4(E_K - V_m) + I_{in},$$

where  $C_m$  is the membrane capacitance,  $g_\ell$  and  $E_\ell$  are the leak conductance and reversal potential,  $\bar{g}_{Na}$  and  $\bar{g}_K$  the maximum conductance,  $E_{Na}$  and  $E_K$  the reversal potentials of the sodium and potassium channels and  $I_{in}$  is the input.

The dynamics of the voltage dependent gating variables can be described by

$$\dot{x} = x_\infty(V_m) - \tau_x(V_m) \dot{x},$$

where the steady state  $x_\infty$  and the time constant  $\tau_x$  are both voltage dependent for  $x \in \{m, n, h\}$ . The variable  $x$  describes the fraction of gating particles in the corresponding channel type that are in the open state. An alternative equivalent formulation that might be more intuitive is

$$\dot{x} = \alpha_x(V_m)(1 - x) - \beta_x(V_m)x,$$

which uses the voltage dependent opening rate  $\alpha_x(V_m)$  and the closing rate  $\beta_x(V_m)$ . Thus, the first term corresponds to the fraction of particles in the closed state  $(1 - x)$  that opens with rate  $\alpha_x(V_m)$ . Similarly, the second term corresponds to the fraction of particles in the open state  $x$  that close with rate  $\beta_x(V_m)$ . The steady state of the gating variable is then  $x_\infty(V_m) = \alpha_x(V_m)/(\alpha_x(V_m) + \beta_x(V_m))$  and the time constant  $\tau_x(V_m) = 1/(\alpha_x(V_m) + \beta_x(V_m))$ .

The Hodgkin-Huxley model can be used to describe different types of neurons in different parts of the brain with the parameters fitted to experimental data of patch clamp recordings. In this study, we use two sets of parameters fitted to cortical and hippocampal pyramidal neurons. The cortical parameters, where taken from Gerstner et al., 2014, with  $m$  and  $h$  fitted by Mainen et al., 1995, on experiments reported by Huguenard, Hamill, and Prince, 1988, and  $h$  fitted by Richard Naud on experiments reported by Hamill, Huguenard, and Prince, 1991. For the hippocampal parameters we relied on an adaptation by Brette et al., 2007, of the model by Traub and Miles, 1991.

### 4.2 Simulations

For our experiments we simulate the Hodgkin-Huxley model with different parameters. We rely on the `brian2` package (Stimberg, Brette, and Goodman, 2019), for the simulation of differential equations in

the context of neuronal data. We use two sets of parameters that were fitted to experimental data, one to cortical pyramidal cells and one to hippocampal pyramidal cells, as described (parameters in SI). For our SBI analysis, we focused on the parameter space in the proximity of the cortex model. We perform simulations similar to the experiments by Köndgen (Köndgen et al., 2008), and inject a sinusoidal input current with Ornstein-Uhlenbeck noise into the neurons membrane:

$$I_{\text{in}} = I_0 + I_1 \sin(2\pi ft) + I_{\text{noise}},$$

where

$$\frac{I_{\text{noise}}(t + dt) - I_{\text{noise}}(t)}{dt} = -\frac{1}{\tau_{\text{noise}}} I_{\text{noise}}(t) + \sigma \sqrt{\frac{2}{dt \tau_{\text{noise}}}} \mathcal{N}(0, 1)$$

is an Ornstein-Uhlenbeck process with time constant  $\tau_{\text{noise}}$ , variance  $\sigma^2$  and normal distribution with zero mean and unit variance  $\mathcal{N}(0, 1)$ . Thus, the input current is sinusoidal with mean  $I_0$ , amplitude  $I_1$  and the noise amplitude is controlled by  $\sigma$  while keeping  $\tau_{\text{noise}} = 10$  ms constant. During the simulation, the refractory period is defined by  $m > 0.5$ , where the input current is not integrated into the neuron's membrane potential. During experiments, we keep  $I_1 = 0.01$  nA and  $\sigma = 0.02$  nA fixed. The simulation length is usually 2 s, of which the first second is considered for initialization and discarded.

The response of the neuron to the input current is examined by analysing the spike times of the membrane potential. Here, we compute the number of spikes after each simulation and define the spike time using the maxima of the action potential. To estimate the output firing rate  $r_{\text{out}}$  of a neuron, the peristimulus time histogram (PSTH) is computed over repeated trials, usually for 100 bins. For each trial, the simulation is repeated with identical parameters but different noise. For simplicity, we run one simulation with multiple identical neurons, that receive the same signal but different noise and that have no interconnections.

For the random-like signals in Fig. 4, we use a combination of different frequencies and amplitudes. By choosing the frequencies involved, we can illustrate some of the neurons feature as the resonance frequency, while showing a clear advance for low frequencies. For the first signal, that should demonstrate the advance for slow frequencies, we chose frequencies  $f_1 = 0.5$ ,  $f_2 = 2$  and  $f_3 = 3$  Hz with amplitudes  $a_1 = -1$ ,  $a_2 = -0.5$  and  $a_3 = 0.1$ . The second signal is more interesting and contains a wider range of frequencies:  $f_1 = 1.5$ ,  $f_2 = 2.4$ ,  $f_3 = 3.3$ ,  $f_4 = 4.5$  and  $f_5 = 4.7$  Hz with amplitudes  $a_1 = 0.5$ ,  $a_2 = 0.4$ ,  $a_3 = 0.3$ ,  $a_4 = 0.4$  and  $a_5 = 0.5$ . The third signal is the same as the first but additionally contains a frequency close to the resonance with  $f_4 = 11$  but with a low amplitude of  $a_4 = 0.02$  that will lead to an over-expressed response in the output rate because of the resonance. The final modulation of the input rate is then a combination of all components and set to be zero mean and unit variance over time:

$$s^*(t) = \sum_i a_i \sin(2\pi f_i t) \quad (6)$$

$$s(t) = \frac{(s^*(t) - \mathbb{E}[s^*])}{\text{Var}[s^*]}. \quad (7)$$

With the expected value  $\mathbb{E}$  and variance  $\text{Var}$  computed over time. The input is then  $I_{\text{in}} = I_0 + I_1 s + I_{\text{noise}}$ . To get a precise estimate of the instantaneous firing rate  $r_{\text{out}}$ , we simulate 10,000,000 trials and compute the PSTH with 1,000 bins.

For the theoretic adaptation models shown in Fig. 5, we use an excerpt of the second signal described above and shown in Fig. 4d and e. For the Hodgkin-Huxley model, we use the cortical parameters for the variables  $m_\infty$ ,  $h_\infty$  and  $\tau_h$  as well as to simulate  $m$  and  $h$ . We obtain the voltage  $v$  via the leaky integrator dynamics  $C_m \dot{v} = g_\ell (E_\ell - v) + I_{\text{in}}$ , where we use again the Hodgkin-Huxley cortex parameters and  $I_{\text{in}} = I_0 + I_1 s$ , with the signal  $s$  as described above, the mean input  $I_0$  set such that the mean of  $v$  is  $-60$  mV and  $I_1$  set such that the amplitude of  $v$  is 2.5 mV for a signal with amplitude 1. To obtain the rate  $r_{\text{HH}}$  from the sodium conductance  $g_{\text{Na}}$ , we need a neuronal activation function. We chose a softplus function, a rectifying function that goes to zero for small and negative values and is linear in the positive regime of large numbers, of the form  $\varphi(x) = \frac{1}{\beta} \log(1 + \exp(\beta(ax + b)))$ . Here,  $\beta = 1$  defines the sharpness of the transition from zero to linear, while we use  $a = 5 \times 10^4$  and  $b = -5$  to shift the sodium conductance such that we get reasonable output rates.

For the threshold adaptation, we have more freedom to choose parameters and variables. Yet, to consider dynamics that are to some extent biologically plausible, we rely on adaptations of the Hodgkin-Huxley variables. For the adaptation we consider, the threshold should increase when the voltage increases. This is the case for  $m_\infty$ , which is a sigmoidal and has a strictly positive derivative. Shifting the sigmoidal and adapting for a smaller slope, we write the steady state of the threshold as

$$v_\infty(v) = v_0 + \frac{\Delta_\vartheta}{1 + \exp(-2 \frac{(v - E_\vartheta)}{\Delta_\vartheta})}, \quad (8)$$

with the minimum  $v_0 = -55$  mV, the slope factor  $\Delta_\vartheta = 30$  mV and the reversal point  $E_\vartheta = -60$  mV. As time constant  $\tau_\vartheta$ , we scale  $\tau_m$  such that  $\tau_r^\vartheta$  in Eq. (2) is 100 ms for the mean voltage  $v_0 = -60$  mV. Again, we consider a softplus function to map the distance to the threshold  $v_\vartheta$  to the output rate. The parameters are  $\beta = 0.1$ ,  $a = 1 \times 10^4$  and  $b = 125$ .

### 4.3 Simulation-based inference

To understand how the parameters of the Hodgkin-Huxley model affect the phase response of a neuron, we use the simulation-based inference (SBI) package (Tejero-Cantero et al., 2020). We define a prior distribution  $p(\theta)$  for each parameter, a Gaussian distribution centered around the respective fit to cortical neurons (Fig. 1). Next, we sample from the priors and run simulation from which we get a phase shift  $x$  for each set of parameters, which allows us to sample the likelihood  $p(x|\theta)$ . Given the priors and the simulations, we use SBI to estimate a posterior distribution  $p(\theta|x)$  using neural density estimation (Tejero-Cantero et al., 2020). To simplify the parametrization we use scaling factors  $\lambda$  as SBI parameters  $\theta$ . While we could directly sample the parameters of the model (e.g.  $g_\ell$ ), the equations for the gating variables (e.g.  $\alpha_m$ ) have multiple parameters themselves and using a single scaling factor here reduces the complexity of the parameter space significantly. To follow a consistent approach, we therefore use scaling factors for all parameters and equations. Explicitly, for the scaling factors, we sample exponents from a normal distribution  $\theta_i \sim \mathcal{N}(0, 0.1)$  such that we get  $\lambda_i = 10^{\theta_i}$ , to account for the multiplicative nature of scaling factors. To get an intuition of how the scaling factors change the gating variables see Fig. SI.1 (SI).

For the observation quantity  $x$  we use the phase shift between  $I_{\text{in}}$  and  $r_{\text{out}}$ . We inject a sinusoidal input current with a frequency of 10 Hz into the neuron and estimate the shift with a sinusoidal fit as described above. For each sampled set of parameters, we run 10,000 repeated trials to obtain an accurate estimate of  $r_{\text{out}}$ . The mean input current  $I_0$  is adapted so that the average  $r_{\text{out}}$  is 10 Hz. Therefore, we inject a constant current into the neuron that we progressively increase until the inter-spike interval is 100 ms. The average firing rate of constant input matches the average firing rate of a 10 Hz sinusoidal input well. In the process, we reject sets of parameters that do not lead to action potentials. Additionally, we reject sets of parameters for which we don't find an input current that leads to an average firing rate between 5 Hz to 15 Hz, which is usually a sign of a broken spike generation mechanism because of a bad parameter combination. To make parameter sampling more efficient, we update and restrict the prior every 1,000 sets of parameters using a feature of the SBI package. In total, we sample 10,000 sets of parameters for the SBI analysis from which 982 sets were discarded, mostly before the first restriction of the prior.

The posterior distribution can be conditioned on any observation or phase shift  $x_o$ , such that we can sample parameters  $\theta_o \sim p(\theta|x_o)$ . Running simulations of Hodgkin-Huxley neurons with the parameters  $\theta_o$  should yield the phase shift  $x_o$  that was used to condition the posterior. Otherwise, either the model is not capable of producing the desired phase shift or the inference step is flawed. With this posterior check, we sample 1000 sets of parameters for each condition and show that the model we use can reproduce the phase shifts we conditioned on (Fig. 2j). Visualizing the conditional posterior distribution, allows us to analyse how the parameters change between different conditions. For the conditional posterior plot, either one or two parameters are varied, while all other parameters are fixed, resulting in either a 1-dimensional or 2-dimensional distribution (Fig. 2k). Here, we use a maximum likelihood approach to set the fixed parameters to the maxima of the conditional posterior distribution. We show in total three different conditional posteriors, each with a different color and the transparency reflecting the probability.

For the individual simulations shown in Fig. 2a-i, for each temporal shift we chose one set of parameter that is typical, i.e., a random representative of the posterior. The parameters are  $\lambda_{g_\ell} = 1.6261$ ,  $\lambda_{\alpha_m} = 0.5310$  and  $\lambda_{\beta_h} = 0.4266$  for the prospective condition (green),  $\lambda_{g_\ell} = 0.7057$ ,  $\lambda_{\alpha_m} = 0.4572$  and  $\lambda_{\beta_h} = 0.3331$  for the instantaneous condition (blue) and  $\lambda_{g_\ell} = 0.4295$ ,  $\lambda_{\alpha_m} = 0.3344$  and  $\lambda_{\beta_h} = 0.3400$  for the retrospective condition (orange).

We used the posteriors to determine which parameters of the Hodgkin-Huxley model are relevant for temporal processing. The posterior distributions of some of the parameters ( $\bar{g}_K$ ,  $\alpha_n$  and  $\beta_n$ ) cover most of the sampling space, indicating that they are not relevant as changing them has little influence on the outcome. For some parameters ( $\bar{g}_{Na}$ ,  $\alpha_h$ ), the posterior distributions of both the prospective and retrospective conditions overlap, such that a change of these parameters is compatible with both. Such parameters cannot be used to distinguish between the two posterior conditions and are hence considered irrelevant to the mechanism of interest. Additionally, we omit  $\beta_m$  as one of the relevant parameters, as it shows a linear dependency with  $\alpha_m$  indicating that the two parameters are correlated and have the same informative value. In the case of the steady states and time constants of the gating variables shown in Fig. 2l-o, we plot the mean over parameters and their standard deviation within each posterior distribution. We consider the same parameters that were used to obtain the distribution of phase shifts shown in Fig. 2j.

## 4.4 Signal analysis

Following Kondgen et al., 2008, the response of a neuron  $r_{out}$  can be described in the linear regime by

$$r(t) \cong r_0 + r_1(f) \sin(2\pi ft + \Phi(f)),$$

where the amplitude response  $r_1(f)$  and the phase response  $\Phi(f)$  are frequency dependent. If not otherwise stated, we chose the mean input current  $I_0$  such that the mean output firing rate of the neuron  $r_0$  is approximately 10 Hz.

To estimate the amplitude and frequency response of a neuron to sinusoidal input, we fit a sinusoidal function to the output rate. In Fig. 1a and b, the shift between the sinusoidal input and the sinusoidal fit of the output rate is shown. Even though the response of a neuron can be non-linear, we expect the temporal shift to be well estimated by a sinusoidal fit, as maxima of the fit will coincide with the maxima of the output rate for a least square fit. Of the 1 s interval that is used for the fit of the sinusoidal, only 0.2 s are shown for illustration.

For the cross-correlogram plot in Fig. 3b and c, we compute the cross-correlation between two spike trains with the `scipy` package (Virtanen et al., 2020) via

$$c(k) = (x * y)(k - N + 1) = \sum_{l=0}^{N-1} x_l y_{l-k+N-1}^*. \quad (9)$$

Because we use a discrete cross-correlation, we discretize the spike times into bins of  $dt = 10^{-4}$  with each element of the array being one when a spike occurred and zero otherwise. When the signal is not sinusoidal, we use the maximum of the cross-correlation as an estimate of the temporal shift between two signals as in Fig. 4.

## References

- Brea, J. et al. (June 2016). “Prospective Coding by Spiking Neurons”. en. In: *PLOS Computational Biology* 12.6. Publisher: Public Library of Science, e1005003. ISSN: 1553-7358. DOI: 10.1371/journal.pcbi.1005003. URL: <https://journals.plos.org/ploscompbiol/article?id=10.1371/journal.pcbi.1005003> (visited on 05/23/2024).
- Senn, W. et al. (Apr. 2024). “A neuronal least-action principle for real-time learning in cortical circuits”. en. In: *eLife* 12. Publisher: eLife Sciences Publications Limited. DOI: 10.7554/eLife.89674.2. URL: <https://elifesciences.org/reviewed-preprints/89674> (visited on 05/21/2024).

- Haider, P. et al. (2021). “Latent Equilibrium: A unified learning theory for arbitrarily fast computation with arbitrarily slow neurons”. In: *Advances in Neural Information Processing Systems*. Vol. 34. Curran Associates, Inc., pp. 17839–17851. URL: <https://proceedings.neurips.cc/paper/2021/hash/94cddb84e8e1de8a725fa2ed61498a4-Abstract.html> (visited on 12/07/2022).
- Ellenberger, B. et al. (Mar. 2024). *Backpropagation through space, time, and the brain*. arXiv:2403.16933 [cs, eess, q-bio]. DOI: 10.48550/arXiv.2403.16933. URL: <http://arxiv.org/abs/2403.16933> (visited on 04/02/2024).
- Köndgen, H. et al. (Sept. 2008). “The Dynamical Response Properties of Neocortical Neurons to Temporally Modulated Noisy Inputs In Vitro”. In: *Cerebral Cortex* 18.9, pp. 2086–2097. ISSN: 1047-3211. DOI: 10.1093/cercor/bhm235. URL: <https://doi.org/10.1093/cercor/bhm235> (visited on 12/08/2022).
- Fuhrmann, G., H. Markram, and M. Tsodyks (Aug. 2002). “Spike frequency adaptation and neocortical rhythms”. eng. In: *Journal of Neurophysiology* 88.2, pp. 761–770. ISSN: 0022-3077. DOI: 10.1152/jn.2002.88.2.761.
- Pozzorini, C. et al. (July 2013). “Temporal whitening by power-law adaptation in neocortical neurons”. en. In: *Nature Neuroscience* 16.7, pp. 942–948. ISSN: 1546-1726. DOI: 10.1038/nn.3431. URL: <https://www.nature.com/articles/nn.3431> (visited on 02/01/2024).
- Lundstrom, B. N. et al. (Nov. 2008). “Fractional differentiation by neocortical pyramidal neurons”. en. In: *Nature Neuroscience* 11.11, pp. 1335–1342. ISSN: 1546-1726. DOI: 10.1038/nn.2212. URL: <https://www.nature.com/articles/nn.2212> (visited on 02/01/2024).
- Tejero-Cantero, A. et al. (Aug. 2020). “sbi: A toolkit for simulation-based inference”. In: *Journal of Open Source Software* 5, p. 2505. DOI: 10.21105/joss.02505.
- Mainen, Z. F. et al. (Dec. 1995). “A model of spike initiation in neocortical pyramidal neurons”. en. In: *Neuron* 15.6, pp. 1427–1439. ISSN: 08966273. DOI: 10.1016/0896-6273(95)90020-9. URL: <https://linkinghub.elsevier.com/retrieve/pii/0896627395900209> (visited on 12/14/2022).
- Traub, R. D. and R. Miles (May 1991). *Neuronal Networks of the Hippocampus*. 1st ed. Cambridge University Press. ISBN: 9780521364812 9780521063319 9780511895401. DOI: 10.1017/CB09780511895401. URL: <https://www.cambridge.org/core/product/identifier/9780511895401/type/book> (visited on 01/30/2024).
- Brette, R. et al. (Dec. 2007). “Simulation of networks of spiking neurons: A review of tools and strategies”. en. In: *Journal of Computational Neuroscience* 23.3, pp. 349–398. ISSN: 1573-6873. DOI: 10.1007/s10827-007-0038-6. URL: <http://link.springer.com/10.1007/s10827-007-0038-6> (visited on 12/08/2022).
- Linaro, D., I. Biró, and M. Giugliano (2018). “Dynamical response properties of neocortical neurons to conductance-driven time-varying inputs”. en. In: *European Journal of Neuroscience* 47.1, pp. 17–32. ISSN: 1460-9568. DOI: 10.1111/ejn.13761. URL: <https://onlinelibrary.wiley.com/doi/abs/10.1111/ejn.13761> (visited on 05/23/2024).
- Hutcheon, B. and Y. Yarom (May 2000). “Resonance, oscillation and the intrinsic frequency preferences of neurons”. In: *Trends in Neurosciences* 23.5, pp. 216–222. ISSN: 0166-2236. DOI: 10.1016/S0166-2236(00)01547-2. URL: <https://www.sciencedirect.com/science/article/pii/S0166223600015472> (visited on 05/23/2024).
- Ostojic, S. et al. (May 2015). “Neuronal Morphology Generates High-Frequency Firing Resonance”. en. In: *Journal of Neuroscience* 35.18, pp. 7056–7068. ISSN: 0270-6474, 1529-2401. DOI: 10.1523/JNEUROSCI.3924-14.2015. URL: <https://www.jneurosci.org/lookup/doi/10.1523/JNEUROSCI.3924-14.2015> (visited on 01/08/2023).
- Hodgkin, A. L. and A. F. Huxley (1952). “A quantitative description of membrane current and its application to conduction and excitation in nerve”. en. In: *The Journal of Physiology* 117.4. eprint: <https://onlinelibrary.wiley.com/doi/pdf/10.1113/jphysiol.1952.sp004764>, pp. 500–544. ISSN: 1469-7793. DOI: 10.1113/jphysiol.1952.sp004764. URL: <https://onlinelibrary.wiley.com/doi/abs/10.1113/jphysiol.1952.sp004764> (visited on 12/08/2022).
- Gerstner, W. et al. (July 2014). *Neuronal Dynamics: From Single Neurons to Networks and Models of Cognition*. 1st ed. Cambridge University Press. ISBN: 9781107060838 9781107635197 9781107447615. DOI: 10.1017/CB09781107447615. URL: <https://www.cambridge.org/core/product/identifier/9781107447615/type/book> (visited on 01/30/2024).



- Huguenard, J. R., O. P. Hamill, and D. A. Prince (Mar. 1988). “Developmental changes in Na<sup>+</sup> conductances in rat neocortical neurons: appearance of a slowly inactivating component”. eng. In: *Journal of Neurophysiology* 59.3, pp. 778–795. ISSN: 0022-3077. DOI: 10.1152/jn.1988.59.3.778.
- Hamill, O. P., J. R. Huguenard, and D. A. Prince (Jan. 1991). “Patch-Clamp Studies of Voltage-Gated Currents in Identified Neurons of the Rat Cerebral Cortex”. en. In: *Cerebral Cortex* 1.1, pp. 48–61. ISSN: 1047-3211, 1460-2199. DOI: 10.1093/cercor/1.1.48. URL: <https://academic.oup.com/cercor/article-lookup/doi/10.1093/cercor/1.1.48> (visited on 12/14/2022).
- Stimberg, M., R. Brette, and D. F. Goodman (Aug. 2019). “Brian 2, an intuitive and efficient neural simulator”. In: *eLife* 8. Ed. by F. K. Skinner et al. Publisher: eLife Sciences Publications, Ltd, e47314. ISSN: 2050-084X. DOI: 10.7554/eLife.47314. URL: <https://doi.org/10.7554/eLife.47314> (visited on 05/20/2024).
- Virtanen, P. et al. (Mar. 2020). “SciPy 1.0: fundamental algorithms for scientific computing in Python”. en. In: *Nature Methods* 17.3, pp. 261–272. ISSN: 1548-7091, 1548-7105. DOI: 10.1038/s41592-019-0686-2. URL: <https://www.nature.com/articles/s41592-019-0686-2> (visited on 05/21/2024).

## SI Supplementary Information

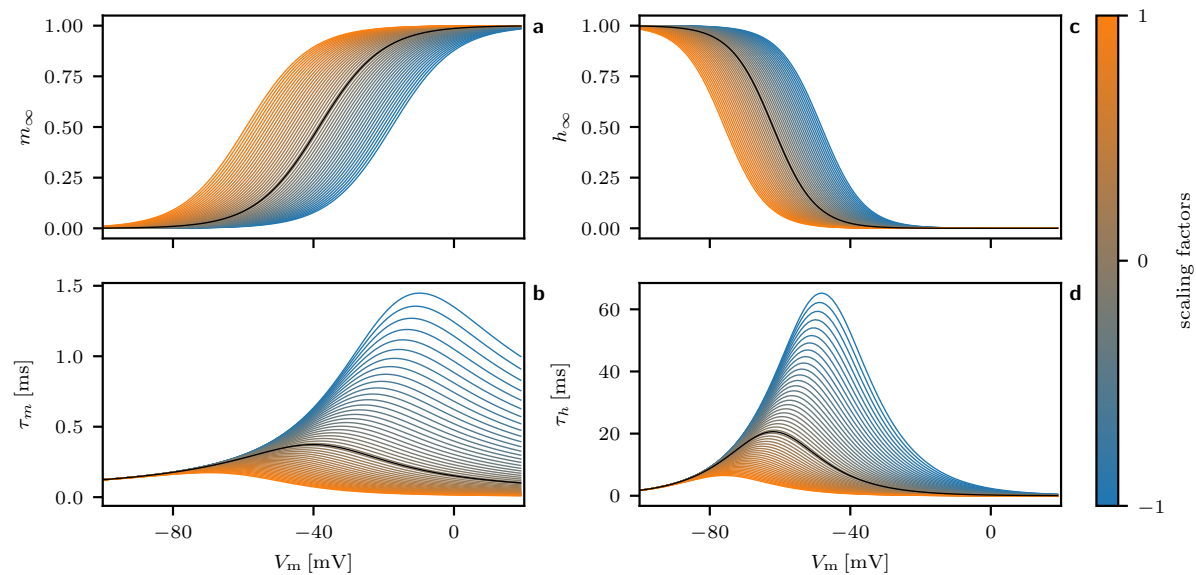


Figure SI.1: Impact of scaling factors  $\lambda$  on the gating variables, where the scaling factors are on a log 10 scale resulting in a range from 1/10 to 10. **(a, b)** show the same results for the impact of  $\beta_h$  on  $h_\infty$  and  $\tau_h$ . **(c, d)** show how  $m_\infty$  and  $\tau_m$  are changed when  $\alpha_m$  is scaled. The black line corresponds to the original variable.

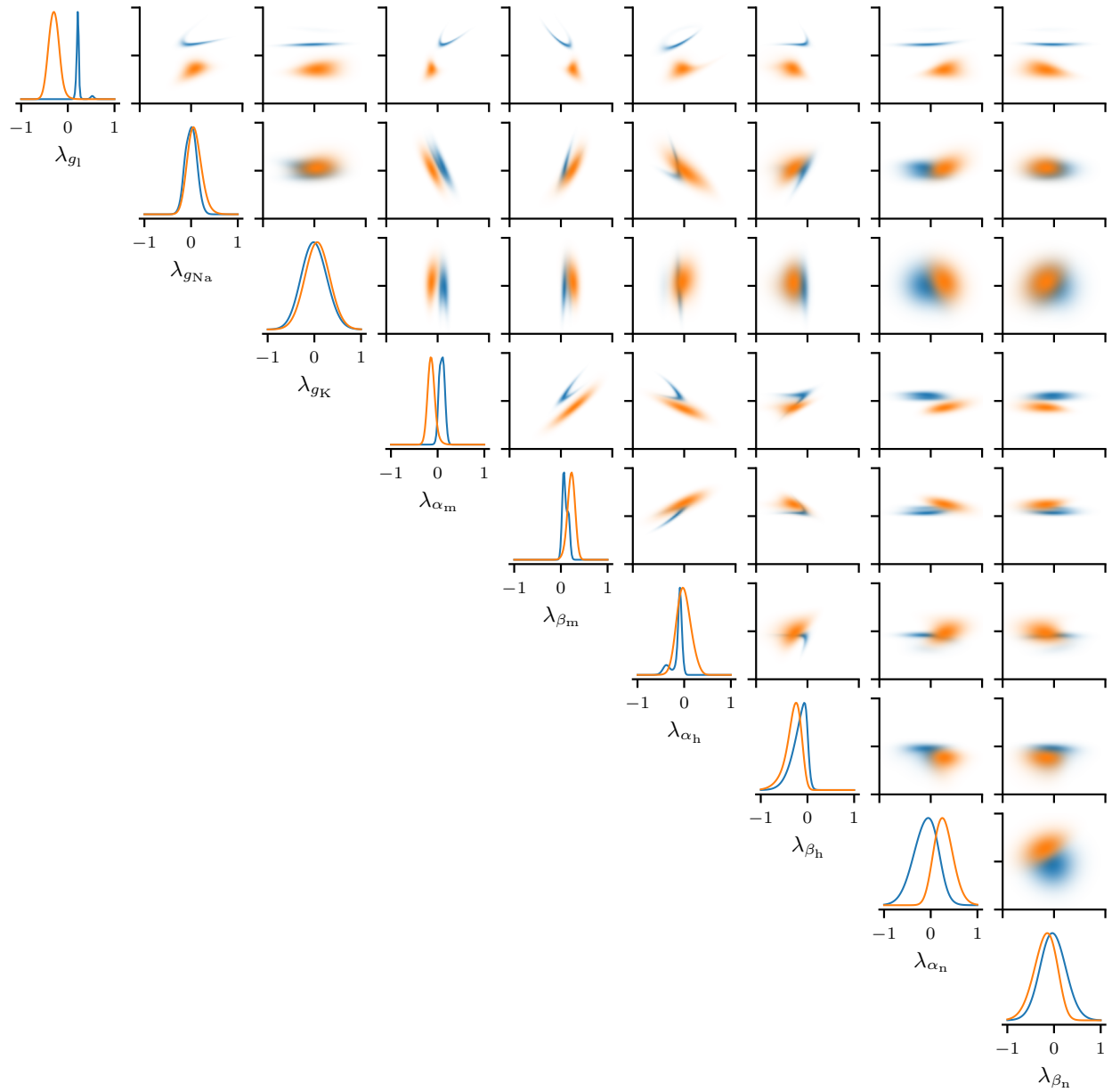


Figure SI.2: 9-dimensional conditional posterior stemming from SBI analysis of the Hodgkin-Huxley model around the cortical parameters. See Methods for a definition of the associated parameters and also Fig. 2 for a detailed description of a similar plot.

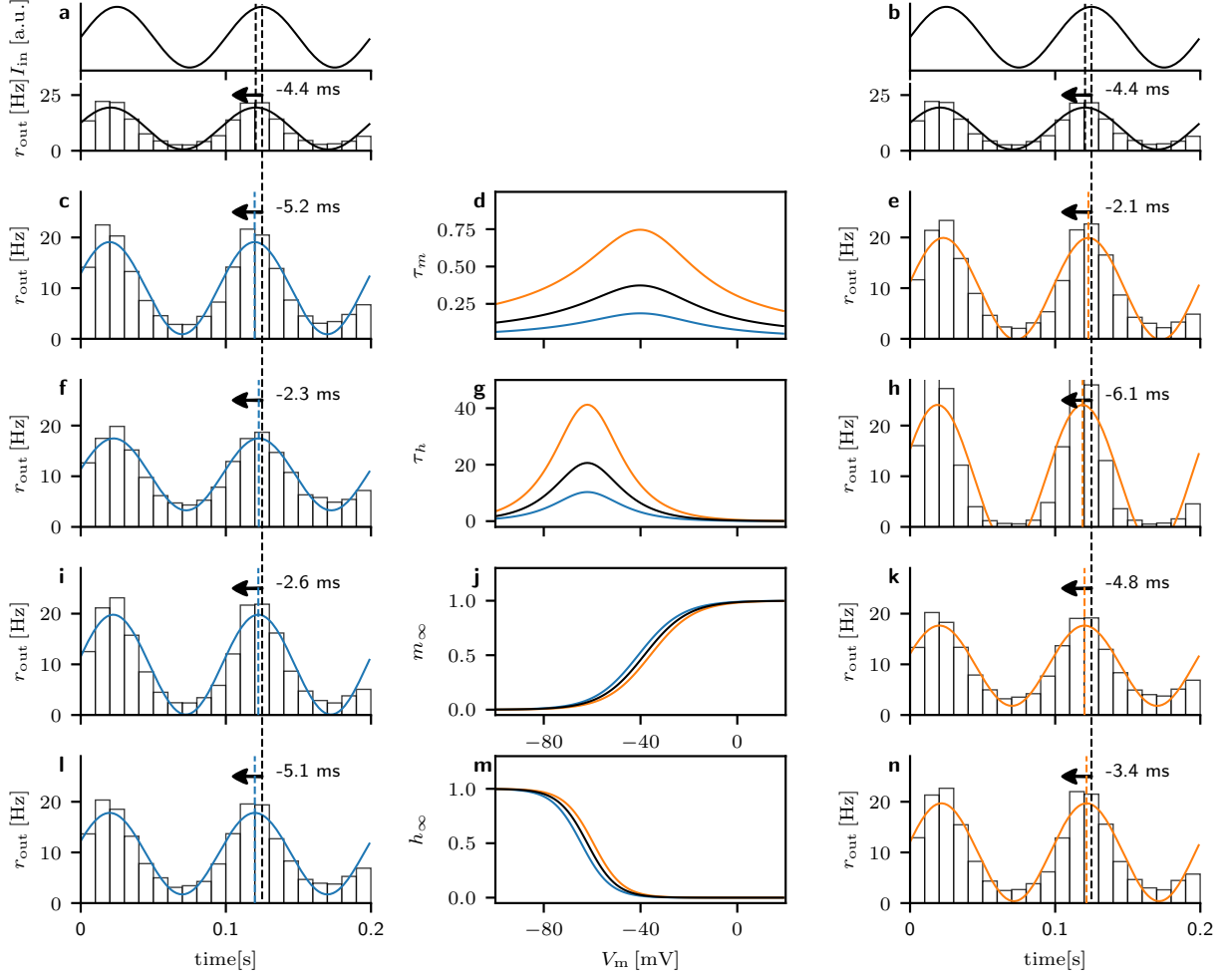


Figure SI.3: With a different notation, the gating variables can be change individually: the steady states can be shifted along the x-axis and the time constants can be scaled along the y-axis. This way, the influence of the steady states and time constants can be analysed independently. **(a, b)** The cortical model of Fig. 1 as reference. **(c-e)** With a smaller  $\tau_m$  the phase advance gets larger (c), while a larger  $\tau_m$  leads to a smaller advance (e) as compared to the original parameters (a). **(f-h)** The opposite is observed for  $\tau_h$ , with a higher  $\tau_h$  leading to a larger advance. **(i-k)** The results shifting  $m_\infty$  2.5 mV to the left leading to a smaller phase advance and to the right resulting in a larger phase advance of  $r_{\text{out}}$  with respect to  $I_{\text{in}}$  as compared to the original model (a, b). **(l-n)** Shifting  $h_\infty$  gives the opposite results.

## SI.1 Hodgkin-Huxley models

$$C_m \dot{v} = g_\ell (E_\ell - v) + \bar{g}_{\text{Na}} m^3 h (E_{\text{Na}} - v) + \bar{g}_{\text{K}} h^4 (E_{\text{K}} - v) + I_{\text{in}} \quad (10)$$

$$I_{\text{in}} = I_0 + I_1 \sin(2\pi f t) + I_{\text{noise}} \quad (11)$$

$$\frac{I_{\text{noise}}(t + dt) - I_{\text{noise}}(t)}{dt} = -\frac{1}{\tau_{\text{noise}}} I_{\text{noise}}(t) + \sigma \sqrt{\frac{2}{dt \tau_{\text{noise}}}} \mathcal{N}(0, 1) \quad (12)$$

$$\frac{m(t + dt) - m(t)}{dt} = \alpha_m (1 - m(t)) - \beta_m m(t) \quad (13)$$

$$\frac{h(t + dt) - h(t)}{dt} = \alpha_h (1 - h(t)) - \beta_h h(t) \quad (14)$$

$$\frac{n(t + dt) - n(t)}{dt} = \alpha_n (1 - n(t)) - \beta_n n(t) \quad (15)$$

### SI.1.1 Cortical Parameters

For  $v$  in mV

$$C_m = 1 \mu\text{F}/\text{cm}^2 \quad (16)$$

$$g_\ell = 3 \times 10^{-4} \text{S}/\text{cm}^2 \quad (17)$$

$$E_\ell = -65 \text{mV} \quad (18)$$

$$E_K = -77 \text{mV} \quad (19)$$

$$E_{\text{Na}} = 55 \text{mV} \quad (20)$$

$$\bar{g}_{\text{Na}} = 40 \text{mS}/\text{cm}^2 \quad (21)$$

$$\bar{g}_K = 35 \text{mS}/\text{cm}^2 \quad (22)$$

$$\alpha_n = 0.02 (v - 25)/(1 - \exp((25 - v)/9)) \quad (23)$$

$$\beta_n = -0.002 (v - 25)/(1 - \exp((v - 25)/9)) \quad (24)$$

$$\alpha_m = 0.182 (v + 35)/(1 - \exp(-(35 + v)/9)) \quad (25)$$

$$\beta_m = -0.124 (v + 35)/(1 + \exp((35 + v)/9)) \quad (26)$$

$$\alpha_h = 0.25 \exp(-(v + 90)/12) \quad (27)$$

$$\beta_h = 0.25 \exp((v + 62)/6)/\exp((v + 90)/12) \quad (28)$$

### SI.1.2 Hippocampal parameters

Again,  $v$  in mV

$$C_m = 1 \mu\text{F}/\text{cm}^2 \quad (29)$$

$$g_\ell = 5 \times 10^{-5} \text{S}/\text{cm}^2 \quad (30)$$

$$E_\ell = -60 \text{mV} \quad (31)$$

$$E_K = -90 \text{mV} \quad (32)$$

$$E_{\text{Na}} = 50 \text{mV} \quad (33)$$

$$\bar{g}_{\text{Na}} = 100 \text{mS}/\text{cm}^2 \quad (34)$$

$$\bar{g}_K = 30 \text{mS}/\text{cm}^2 \quad (35)$$

$$v_T = -63 \text{mV} \quad (36)$$

$$\alpha_m = 0.32 (13 - v + v_T)/(\exp((13 - v + v_T)/4) - 1) \quad (37)$$

$$\beta_m = 0.28 (v - v_T - 40)/(\exp((v - v_T - 40)/5) - 1) \quad (38)$$

$$\alpha_h = 0.128 \exp((17 - v + v_T)/18) \quad (39)$$

$$\beta_h = 4/(1 + \exp((40 - v + v_T)/5)) \quad (40)$$

$$\alpha_n = 0.032 (15 - v + v_T)/(\exp((15 - v + v_T)/5) - 1) \quad (41)$$

$$\beta_n = 0.5 \exp((10 - v + v_T)/40) \quad (42)$$